A Multiphase Solute Diffusion Model for Dendritic Alloy Solidification

C.Y. WANG and C. BECKERMANN

A solute diffusion model, aimed at predicting microstructure formation in metal castings, is proposed for dendritic solidification of alloys. The model accounts for the different length scales existing in a dendritic structure. This is accomplished by utilizing a multiphase approach, in which not only the various physical phases but also phases associated with different length scales are considered separately. The macroscopic conservation equations are derived for each phase using the volume averaging technique, with constitutive relations developed for the interfacial transfer terms. It is shown that the multiphase model can rigorously incorporate the growth of dendrite tips and coarsening of dendrite arms. In addition, the distinction of different length scales enables the inclusion of realistic descriptions of the dendrite topology and relations to key metallurgical parameters. Another novel aspect of the model is that a single set of conservation equations for solute diffusion is developed for both equiaxed and columnar dendritic solidification. Finally, illustrative calculations for equiaxed, columnar, and mixed columnar-equiaxed solidification are carried out to provide quantitative comparisons with previous studies, and a variety of fundamental phenomena such as recalescence, dendrite tip undercooling, and columnar-to-equiaxed transition (CET) are predicted.

I. INTRODUCTION

MODELING of transport phenomena occurring during dendritic alloy solidification has received considerable research attention in the past several decades.[1] Recently, interest has been focusing on an important and promising approach, namely micro-macroscopic modeling. The main goal of this approach is to incorporate descriptions of fundamental microscopic phenomena, such as nucleation, undercooling, and grain growth, into macroscopic heat-flow calculations in order to predict microstructure formation of a solidifying material on the system scale. A review of micro-macroscopic modeling has been provided by Rappaz[2] and recent developments have been reported in conference proceedings.[3]

In an attempt to achieve detailed coupling between micro- and macroscopic phenomena, Ni and Beckermann[4] proposed a two-phase model for mass, momentum, energy, and species transport in a solidifying system. The model is formulated by viewing the solid and liquid phases separately and averaging the field properties of each phase over a representative elementary volume. Through the volume averaging process, phase interaction terms appear in the resulting macroscopic balance equations that reflect the effects of the transport phenomena occurring on the microscopic scale. These interaction terms are all proportional to the solid/liquid interfacial area-per-unit volume, which represents the sole microscopic length scale. The same volume-averaging technique was employed by Ganesan and Poirier[5] to derive macroscopic mass and momentum equations for a stationary solid phase.

Nevertheless, volume-averaged two-phase models are not well suited for incorporating microstructural features present in dendritic solidification. This problem originates from the single-scale averaged description of phase behaviors. In traditional volume averaging, no distinction is made between properties of a phase associated with different microscopic length scales. The phenomena occurring on various microscopic length scales are smeared and modeled using a single mean characteristic length (*i.e.*, the interfacial area concentration). In reality, in dendritic growth there exist at least three disparate microscopic length scales that are smaller than the characteristic size of an averaging volume: (1) the overall size of the crystal or the primary dendrite arm spacing, (2) the secondary dendrite arm spacing, and (3) the radius of a dendrite tip. Obviously, the transport phenomena occurring on the various microscopic scales differ greatly from one another and cannot be well described based on a single mean characteristic length, although they are all taking place within the same averaging volume. In other words, a single-scale model provides insufficient resolution to capture dynamic behaviors on several microscopic length scales. Such resolution is, however, required for the complete incorporation of microscopic effects in a macroscopic model and the prediction of microstructure formation in a solidifying system.

Considerable progress has been made to account for the heterogeneous nature of microstructures in the micro-macroscopic modeling of both equiaxed[6,7,8] and columnar[9,10] dendritic solidification. In the models of equiaxed dendritic growth, the necessary resolution is obtained by viewing the liquid phase in a control volume as two distinct fluids associated with two length scales: the liquid within the dendritic structure and the liquid outside the equiaxed grain. It is then possible to separately account for the different solute diffusion phenomena in the interdendritic structure and the dendrite tip region and, more importantly, to incorporate a growth

C.Y. WANG, Graduate Research Assistant, and C. BECKERMANN, Associate Professor, are with the Department of Mechanical Engineering, The University of Iowa, Iowa City, IA 52242.

Manuscript submitted November 12, 1992.

model for the dendrite tips. Similarly, when analyzing columnar dendritic solidification, Flood and Hunt[9] distinguish between the liquid in the interdendritic region and that outside the columnar front and also take into account the undercooling at the primary dendrite tips.

Although these recent investigations have obtained successful results, they fail to provide a consistent and general framework for micro-macroscopic modeling of dendritic solidification. For example, in Dustin and Kurz's model[6] of equiaxed growth and in Flood and Hunt's model[9] of columnar solidification, the growth model for the dendrite tips is introduced at the expense of not conserving solute outside of the grain envelope or at the columnar front.[2] The same practice was repeated by Kerr *et al.*[11] The only model that not only conserves solute but also incorporates a dendrite-tip-growth model in a rigorous and consistent manner is due to Rappaz and Thevoz.[7] Unfortunately, lengthy calculations are required to obtain the microscopic solute profile outside each equiaxed grain, which limits its utility in a macroscopic model. Although the analytical version of the model[8] is suitable for incorporation into a macroscopic model, it is implied that the average concentration of the liquid outside of the grain remains at its initial value, which may not be valid in some cases (*e.g.*, in the presence of macrosegregation). Finally, none of the previously mentioned micro-macroscopic models accounts for finite-rate solute diffusion in the solid on a microscopic scale.

The aim of this article is to formally and rigorously develop a micro-macroscopic model of dendritic solidification by utilizing a multiphase approach and volume averaging. Moreover, an attempt is made to construct a unified theory for both equiaxed and columnar dendritic solidification. As a first step, this article solely deals with solute diffusion. Due to the large value of the Lewis number for metallic alloys, thermal equilibrium is assumed to prevail on a microscopic scale, while the macroscopic temperature distribution is considered to be known from the solution of the energy equation. The inclusion of melt convection and solid movement is nontrivial and will be covered in a future publication. In the following, the basic model is introduced, and the relevant supplementary relations are provided, with the last two sections focusing on practically useful limiting cases and both qualitative and quantitative comparisons with previous studies.

II. BASIC MODEL CONSIDERATIONS

A. *Multiphase Approach*

Consider a small volume element that contains several equiaxed or columnar dendritic crystals, as schematically illustrated in Figure 1, in which two different interfacial length scales can be distinguished. An interfacial scale (having the unit of length) is defined as the ratio of the volume of the structure to the interfacial area. In the equiaxed case, the solid crystal and the interdendritic liquid share a common interfacial length scale of 10^{-5} to 10^{-4} m, whereas the interface between the liquid outside the grains and the interdendritic liquid has a larger length scale (of the order of 10^{-4} to 10^{-3} m). The same

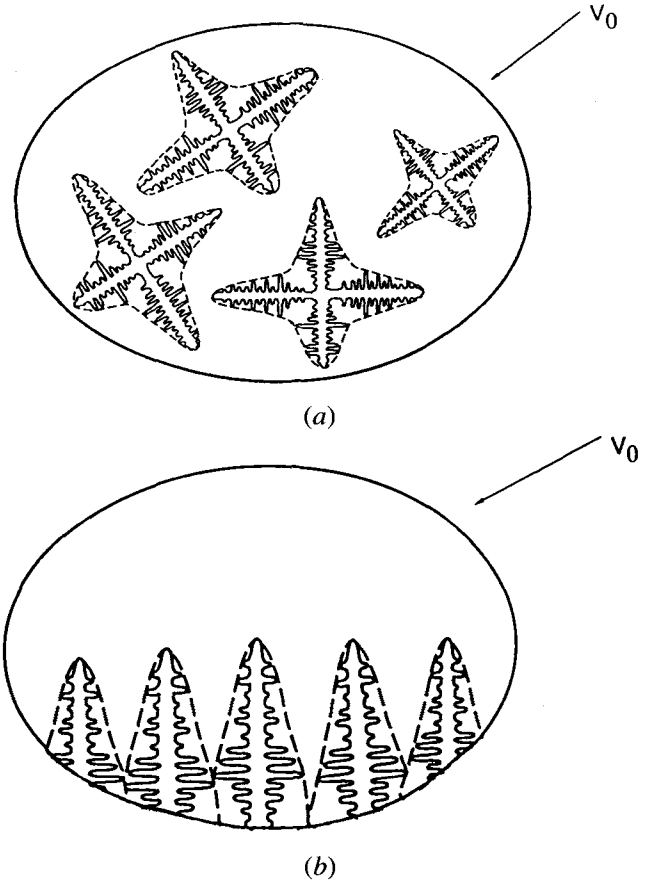

Fig. 1 — Schematic illustration of the averaging volume and the dendrite envelopes (interrupted lines) for (*a*) equiaxed growth and (*b*) columnar growth.

is true for the columnar case, if one notes the difference between the primary and secondary arm spacings (see Figure 1(b)). The size of the volume element is chosen such that it is much larger than all interfacial length scales but small compared to the system scale (of the order of 10^{-1} to 10^{0} m). Hence, a proper volume element could have a radius between 10^{-3} and 10^{-2} m. A volume element of this size is what all macroscopic models are actually based on.

The hypothetical interface between the interdendritic liquid and the liquid outside the crystals is referred to as the dendrite envelope. The specification of this envelope is somewhat subjective. However, a reasonable choice appears to be a smooth surface connecting the primary and secondary dendrite arm tips, as shown by the interrupted line in Figure 1. More details on the envelope topology can be found in Section IV.

Now, the volume element can be considered to consist of three different phases: the solid phase and the two liquid phases. The two liquid phases separated by the dendrite envelope are distinguished by their different interfacial length scales. This multiphase approach to a heterogeneous system is realistic, since a fluid within a structure of a larger scale really could have different macroscopic properties than the same fluid in a smaller scale structure. It has long been recognized that the effective transport properties of a fluid within a microstructure are not only dependent on its physical

properties but also on the geometry of the structure.[12,13,14]

In the multiphase approach, separate macroscopic conservation equations are formulated for each phase. These macroscopic equations are linked through interfacial transfer terms, which reflect the microscopic transport phenomena present at the interfaces. The new interface between the two liquid phases (*i.e.*, the envelope), thus, provides an opportunity to incorporate additional microscopic phenomena in the model and transmit information from the two different length scales into the macroscopic equations. The macroscopic conservation equations are derived using the volume-averaging technique, which is described in Section II–B.

B. *Volume Averaging*

Volume averaging has been a popular technique to derive macroscopic conservation equations for multiphase transport phenomena with and without phase change. In its application to solidification, a number of advantages have been pointed out.[4] Volume averaging shows how the various terms in the macroscopic equations arise and how the resulting macroscopic variables are related to the corresponding microscopic ones. This gives considerable insight into the formulation of constitutive relations for the incorporation of the microscopic phenomena. In this work on heterogeneous solidification systems, volume averaging is also attractive, because it shows how physical phenomena occurring on one length scale are linked to those on another scale in a macroscopic description.

The averaging volume, V_0, is shown in Figure 1. Rigorously, the spatial smoothing of a physical property belonging to the smaller-scale phase over the averaging volume, V_0, requires the knowledge of the transport equations first averaged over a smaller volume. Hence, in order to develop a macroscopic equation for the smaller-scale phase in a heterogeneous system, based on the volume V_0, the microscopic or *point* equation must be spatially averaged successively over two averaging volumes of different size. This is the basic idea underlying the so-called dual-scale volume-averaging technique that was recently developed by Wang and Beckermann.[15] However, the averaging theorems established for that technique reduce identically to those in the conventional volume-averaging method, if it is assumed that the smaller averaging volume is spatially independent (but it can be time dependent) inside the larger volume, V_0. Therefore, for the sake of simplicity, the conventional volume-averaging method is employed here, and each fluid having a distinct length scale is viewed as a separate phase. While the details of the method have been well documented;[16–19] only the averaging theorems are provided in the following:

$$\left\langle \frac{\partial \Psi_k}{\partial t} \right\rangle = \frac{\partial \langle \Psi_k \rangle}{\partial t} - \frac{1}{V_0} \int_{A_k} \Psi_k \mathbf{w} \cdot \mathbf{n} dA \qquad [1a]$$

$$\langle \nabla \Psi_k \rangle = \nabla \langle \Psi_k \rangle + \frac{1}{V_0} \int_{A_k} \Psi_k \mathbf{n} dA \qquad [1b]$$

where the averaging operator and the intrinsic volume average are defined, respectively, as

$$\langle \Psi_k \rangle = \frac{1}{V_0} \int_{V_0} X_k \Psi_k dV \qquad [2a]$$

$$\langle \Psi_k \rangle^k = \frac{1}{V_k} \int_{V_0} X_k \Psi_k dV \qquad [2b]$$

with X_k denoting a phase function, equal to unity in phase k and zero elsewhere, and V_k is the volume of phase k in V_0.

The factor $\mathbf{n}$ in Eqs. [1a] and [1b] denotes the outwardly directed unit vector normal to an interface, and $\mathbf{w}$ is the velocity of the interface. Note that A_k stands for the total interfacial area of the k-phase adjacent to all other phases j; *i.e.*,

$$A_k = \sum_{j, j \neq k} A_{kj} \qquad [3]$$

Equations [1a] and [1b] are utilized in Section II–C to derive the macroscopic transport equations.

C. *Macroscopic Equations*

In the absence of melt convection and solid movement, the relevant equations governing solute diffusion are the statements of mass and solute conservation within each phase. Their microscopic versions can be written as

$$\frac{\partial \rho_k}{\partial t} = 0 \qquad [4]$$

and

$$\frac{\partial}{\partial t} (\rho_k C_k) = -\nabla \cdot \mathbf{j}_k \qquad [5]$$

where $\mathbf{j}_k$ is the diffusive species flux in phase k. Making use of the averaging theorems, Eqs. [1a] and [1b], we obtain the corresponding macroscopic versions as follows:

$$\frac{\partial}{\partial t} (\rho_k \varepsilon_k) = \sum_{j, j \neq k} \Gamma_{kj} \qquad [6]$$

and

$$\frac{\partial}{\partial t} (\rho_k \varepsilon_k \langle C_k \rangle^k) = -\nabla \cdot (\langle \mathbf{j}_k \rangle) + \sum_{j, j \neq k} J_{kj} \qquad [7]$$

where ε_k is the volume fraction of phase k within the averaging volume, Γ_{kj} denotes the net rate of mass exchange of phase k at the k-j interface, and J_{kj} is the species transfer rate of phase k at the k-j interface. The interfacial species transfer rate, J_{kj}, consists of two parts: namely,

$$J_{kj} = J_{kj}^{\Gamma} + J_{kj}^{j} \qquad [8]$$

where the first part is due to interfacial movement and the second arises from species diffusion. Note that the motion of the solid-interdendritic liquid interface is caused by phase change, whereas that of the dendrite

envelope is induced by dendrite tip growth. The volume averaging procedure results in the following explicit relations for the interfacial transfer terms:

$$\Gamma_{kj} = \frac{1}{V_0}\int_{A_{kj}} \rho_k \mathbf{w}\cdot\mathbf{n}\,dA \qquad [9]$$

$$J^{\Gamma}_{kj} = \frac{1}{V_0}\int_{A_{kj}} \rho_k C_k \mathbf{w}\cdot\mathbf{n}\,dA \qquad [10]$$

$$J^{i}_{kj} = -\frac{1}{V_0}\int_{A_{kj}} \mathbf{j}_k\cdot\mathbf{n}\,dA \qquad [11]$$

These terms are constrained by interfacial balances on each k-j interface; *i.e.*,

$$\Gamma_{kj} + \Gamma_{jk} = 0 \qquad [12]$$

and

$$J_{kj} + J_{jk} = 0 \qquad [13]$$

Obviously, an overall interfacial balance follows by summing up the interfacial balances for each interface. The specification of the interfacial transfers in terms of macroscopic variables requires the development of constitutive relations for the system under consideration.

III. BASIC CONSTITUTIVE RELATIONS

Constitutive relations are formulated for a three-phase system consisting of the solid ($k = s$), the interdendritic liquid ($k = d$), and the extradendritic liquid outside the dendrite envelopes ($k = l$), so that $\varepsilon_s + \varepsilon_d + \varepsilon_l = 1$. It is further assumed that the solid (s) has only pointwise contact with the liquid (l) outside the dendrite envelopes, so that

$$A_{sd} = A_{ds} = A_s, \quad A_{dl} = A_{ld} = A_e, \quad \text{and} \quad A_{sl} = A_{ls} = 0 \qquad [14]$$

These geometrical relationships imply that there exists no direct coupling between phases s and l, while phase d interacts with both phases s and l.

A. *Modeling of the Interfacial Transfers Due to Interface Movement*

The exact expressions for the interfacial transfers of mass and species due to interface movement are given by Eqs. [9] and [10]. Using the mean value theorem for integrals, these terms can be modeled as the product of an interfacial area concentration, $S_s = A_s/V_0$ or $S_e = A_e/V_0$, and a mean interfacial flux. Hence, at the s-d interface:

$$\Gamma_{sd} = -\Gamma_{ds} = S_s\rho_s\bar{w}_{ns} \qquad [15]$$

where $\bar{w}_{ns}$ is defined as the average normal velocity of the solid-interdendritic liquid interface, which is solely due to phase change. Similarly, at the d-l interface:

$$\Gamma_{dl} = -\Gamma_{ld} = S_e\rho_d\bar{w}_{ne} \qquad [16]$$

where $\bar{w}_{ne}$ denotes the average normal velocity of the dendrite envelope. As mentioned before, the movement of the envelope is related to the kinetics of the dendrite tips, which is discussed in more detail in Section VI.

In a like manner, the interfacial species transfers due to interface movement can be modeled as

$$J^{\Gamma}_{sd} = \bar{C}_{sd}\Gamma_{sd}; \qquad J^{\Gamma}_{ds} = \bar{C}_{ds}\Gamma_{ds} \qquad [17]$$

for the s-d interface, and

$$J^{\Gamma}_{dl} = \bar{C}_{dl}\Gamma_{dl}; \qquad J^{\Gamma}_{ld} = \bar{C}_{ld}\Gamma_{ld} \qquad [18]$$

for the d-l interface. The overbars denote an average over the interfacial area, A_s or A_e.

B. *Modeling of the Interfacial Species Transfers Due to Diffusion*

The exact expression for the interfacial species transfer due to diffusion, J^{i}_{kj}, is given by Eq. [11]. Physically, this term describes the interfacial diffusion process caused by species concentration gradients. The integral in Eq. [11] can be evaluated again as the product of the interfacial area concentration, S, and a mean interfacial diffusive flux. The flux is directly proportional to its driving force, namely, the difference between the interfacial and volume-averaged concentrations of a phase. On the other hand, the flux is inversely proportional to a so-called solute diffusion length, l, which characterizes the resistance to diffusion. Hence, the following mathematical expressions can be written down:

$$J^{i}_{sd} = S_s\rho_s\frac{D_s}{l_{sd}}(\bar{C}_{sd} - \langle C_s\rangle^s) \qquad [19]$$

and

$$J^{i}_{ds} = S_s\rho_d\frac{D_d}{l_{ds}}(\bar{C}_{ds} - \langle C_d\rangle^d) \qquad [20]$$

for the s-d interface. It should be noted that ρ_d and D_d are not necessarily equal to ρ_l and D_l, respectively, because these properties are functions of the local concentration and temperature. Likewise, one has that

$$J^{i}_{dl} = S_e\rho_d\frac{D_d}{l_{dl}}(\bar{C}_{dl} - \langle C_d\rangle^d) \qquad [21]$$

and

$$J^{i}_{ld} = S_e\rho_l\frac{D_l}{l_{ld}}(\bar{C}_{ld} - \langle C_l\rangle^l) \qquad [22]$$

at the d-l interface.

Figure 2 schematically illustrates the microscopic concentration distributions in the solid, interdendritic, and extradendritic liquid regions. The interfaces depicted in Figure 2 represent infinitesimal sections of the interfaces shown in Figure 1 and are drawn, for simplicity, as straight lines. The physical meanings of the various diffusion lengths, l, are also shown therein. Mathematically, a diffusion length is defined as

$$l_{kj} = \frac{\bar{C}_{kj} - \langle C_k\rangle^k}{-\left.\dfrac{\partial C_k}{\partial n}\right|_{kj}} \qquad [23]$$

where the denominator represents the mean concentration gradient in phase k normal to the kj interface. The diffusion length is generally a complicated function of the microscopic phenomena, and its determination requires a formal microscopic analysis of the diffusion processes in a phase. Several simple analytical results are presented in the Appendix.

C. *Modeling of the Macroscopic Species Fluxes*

In order to model the macroscopic species fluxes, it is assumed that the species diffusion is governed by Fick's law and that the fluctuating components of the density and the mass diffusivity of phase k are negligibly small. Hence,

$$\langle j_k \rangle = -D_k \rho_k \langle \nabla C_k \rangle \qquad [24]$$

Following Ni and Beckermann,[4] Eq. [24] can be rewritten by applying an averaging theorem and introducing an effective mass diffusivity, D_k^*, such that

$$\langle j_k \rangle = -D_k^* \rho_k \varepsilon_k \nabla \langle C_k \rangle^k \qquad [25]$$

where D_k^* is generally different from its microscopic counterpart, D_k. Although we have formally included species diffusion on a macroscopic scale, in practice this term may be negligible, because the solute diffusion length is much smaller than the characteristic length for diffusion into or out of an averaging volume. Mathematically, this can be shown by comparing the magnitudes of the macroscopic diffusion term and the interfacial transfer term due to diffusion in Eq. [7]. Noting that the interfacial area concentration and the diffusion length are proportional to l/d and d, respectively, where d is a representative microscopic length, the ratio of the magnitudes of the two terms is

$$\frac{\nabla(-\langle j_k \rangle)}{J_{kj}} \approx \frac{D_k^* \rho_k \varepsilon_k \Delta C / L^2}{S \rho_k D_k \Delta C / l} \approx \frac{d^2}{L^2} \ll 1 \qquad [26]$$

where L is a macroscopic length and ΔC stands for a suitable concentration scale. The same has been argued by Rappaz and Voller[20] and Poirier *et al.*[21] in different ways.

IV. GEOMETRICAL RELATIONS

The interfacial area concentrations, S_s and S_e, characterize the topology of the interfacial structures and are thus related to complex microscopic phenomena, such as the growth of various solid microstructures, impingement of interfaces, and coarsening of dendrite arms. The area concentrations play important roles in the modeling of the interfacial transfer terms and need to be modeled through supplementary relations, which can be developed from either experiments or certain theoretical considerations. In fact, it has recently been proposed to base micro-macroscopic models directly on the specific surface area, S_v.[22] The inverse of the specific surface area is a more accurate measure of the length scale of a microstructure than the traditionally employed spacings[2] and can easily be measured. The interfacial area concentration, S, is related to S_v by $S = S_v(1 - \varepsilon)$, where

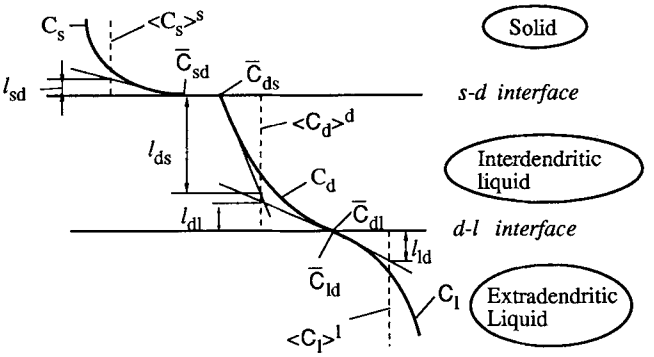

Fig. 2—Illustration of the species diffusion lengths.

ε is the volume fraction of the microstructure under consideration. Hence, once relations for S_v become available, they can be used in the present model.

In the following, a more traditional approach is taken, and an attempt is made to relate the interfacial area concentrations to certain dendrite spacings, the nuclei density, time (through coarsening), and the various volume fractions (which are also functions of time). In the present model, different length scales have been distinguished, and, thus, it is possible to relate the interfacial area concentrations to such metallurgical parameters. This also enables the incorporation of microstructural phenomena (*e.g.*, coarsening) that occur only on a particular length scale.[23] This matter was obscured in a previous two-phase model[4] through the use of mean geometrical parameters for the averaging volume.

A. *Solid/Liquid Interface*

The area concentration of the interface between the solid and the interdendritic liquid can be modeled by assuming a simple one-dimensional platelike geometry of the secondary dendrite arms as shown in Figure A1. This is applicable to both equiaxed and columnar structures and is traditionally adopted in most microscopic analyses. For such a geometry, it is readily shown that

$$d_s = \frac{\varepsilon_s \lambda_2}{1 - \varepsilon_l} \qquad [27]$$

and

$$S_s = \frac{2}{\lambda_2} \qquad [28]$$

Substituting Eq. [27] into Eq. [28], we obtain a relation between S_s and the mean characteristic length (diameter) as

$$S_s = \frac{2\varepsilon_s}{(1 - \varepsilon_l) d_s} \qquad [29]$$

It is interesting to see that this result matches well with the general expressions obtained by DeHoff and Rhines[24] and Bird *et al.*[25] The numerical factor can be adjusted for other choices of the geometry. In addition, we note that Eq. [28] is ready for the incorporation of

the coarsening effect. For example, by using the coarsening law established by Kattamis *et al.*:[26]

$$\lambda_2 = \beta t_a^{1/3} \qquad [30]$$

Eq. [28] gives

$$S_s \sim t_a^{-1/3} \qquad [31]$$

where t_a is the local "aging" time. This result is consistent with the coarsening experiments conducted by Marsh *et al.*[27] at a constant solid fraction.

Note that due to the assumption of a one-dimensional platelike geometry for the solid/liquid interface, the interfacial area concentration, S_s, is not an explicit function of the solid volume fraction (but S_v is; see earlier). This may not be a good approximation during the initial and final stages of solidification when the interface experiences qualitative changes in its topology. This problem can be overcome by using the correction factor for the interfacial area due to Avrami[28] to account for impingement of interfaces or the empirical relation proposed by Speich and Fisher.[29]

B. *Dendrite Envelope*

The area concentration of the dendrite envelope is modeled by introducing an envelope shape factor defined as

$$\phi = A_{\text{equivalent}}/A_{\text{actual}} \qquad [32]$$

By equivalent we mean an equivalent sphere or cylinder of the same volume as the actual crystal envelope. Equiaxed crystal envelopes are most appropriately described by equivalent spheres, while equivalent cylinders are chosen for the columnar case. The shape factors are schematically illustrated in Figures 3(a) and (b). A shape factor always lies between zero and unity, since a sphere and a cylinder have the least possible surface area for three-dimensional and axisymmetric bodies, respectively; however, for envelope shapes similar to the ones shown in Figure 3, ϕ_e is relatively close to unity.[30] If the envelope is shape preserving during growth, ϕ_e can be taken as a constant.

1. *Equiaxed growth*

For equiaxed growth, it can easily be shown that

$$S_e = \frac{1}{\phi_e}\frac{6(1-\varepsilon_l)}{d_e} \qquad [33]$$

Note that this result is consistent with Eq. [29]. In Eq. [33], d_e is the diameter of the equivalent sphere that can be related to the number of crystals per unit volume, n, as

$$d_e = \left(\frac{6(1-\varepsilon_l)}{n\pi}\right)^{1/3} \qquad [34]$$

where n must be calculated from a nucleation model.[2] Substituting Eq. [34] into Eq. [33] results in the following relation for S_e in terms of the nuclei density:

$$S_e = \frac{1}{\phi_e}(36\pi)^{1/3}\, n^{1/3}\,(1-\varepsilon_l)^{2/3} \qquad [35]$$

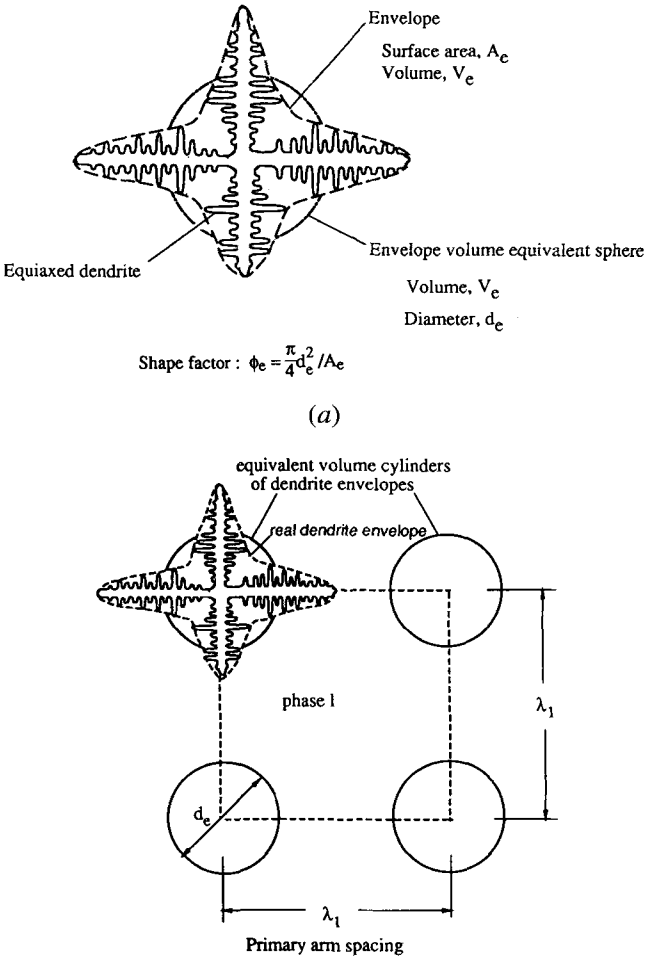

Fig. 3—Schematic of shape factors for (*a*) an equiaxed dendrite envelope and (*b*) a square arrangement of columnar dendrite envelopes.

2. *Columnar growth*

For the equivalent cylinders assumed in columnar growth, we have that

$$S_e = \frac{1}{\phi_e}\frac{4(1-\varepsilon_l)}{d_e} \qquad [36]$$

By assuming a square pattern of the columnar dendrites on a transverse cross section, as shown in Figure 3(b), the equivalent diameter, d_e, can be related to the familiar primary arm spacing, λ_1, such that

$$d_e = \left(\frac{4(1-\varepsilon_l)}{\pi}\right)^{1/2}\lambda_1 \qquad [37]$$

Then, substitution of Eq. [37] into Eq. [36] yields

$$S_e = \frac{1}{\phi_e}(4\pi)^{1/2}\,(1-\varepsilon_l)^{1/2}\frac{1}{\lambda_1} \qquad [38]$$

The primary arm spacing, λ_1, depends mainly on the columnar front velocity and the temperature gradient and can be calculated from an appropriate model.[31] It should be mentioned that Eqs. [37] and [38] are also

valid for other arrangements of the dendrites except for a slight change in the numerical factor.

By comparing Eq. [35] with Eq. [38], it is apparent that the number density of equiaxed crystals, n, can equivalently be viewed as the number density of primary arms in columnar solidification, that is $n^{1/3} \sim 1/\lambda_1$. Furthermore, Eqs. [35] and [38] reveal the following important parametric relation:

$$S_e \sim n^{1/3} \quad \text{or} \quad 1/\lambda_1 \qquad [39]$$

The final equivalent radius ($R_f = d_e/2$) of a dendrite, which is useful in the calculation of the diffusion lengths (Appendix), can be obtained from Eq. [34] or [37] by taking $\varepsilon_l = 0$. Similar to the solid/liquid interface, the envelope area concentrations expressed by Eqs. [35] and [38] need to be modified during the initial and final stages of solidification. In particular, S_e should be equal to zero for $\varepsilon_l = 0$.

V. THERMODYNAMIC RELATIONS

Under the assumption of local thermodynamic equilibrium, the following conditions are valid at the solid/interdendritic liquid interface:

$$\bar{C}_{sd}/\bar{C}_{ds} = \kappa \qquad [40]$$

$$\bar{C}_{ds} = \frac{T - T_m}{m_l} \qquad [41]$$

where we utilize the symbol T without a subscript to represent the single temperature of an averaging volume (Section I).

At the d-l interface, phases d and l are actually the same liquid. Hence,

$$\bar{C}_{dl} = \bar{C}_{ld} = \bar{C}_e \qquad [42]$$

where $\bar{C}_e$ denotes the liquid concentration on the dendrite envelope. The envelope concentration cannot be obtained from the phase diagram but is determined by the interfacial species balance. Substituting Eqs. [16], [18], [21], and [22] into Eq. [13] results in

$$(\bar{C}_{ld} - \bar{C}_{dl})\,\rho_l \bar{w}_{ne} = \rho_l \frac{D_l}{l_{ld}} (\bar{C}_{ld} - \langle C_l \rangle^l) + \rho_d \frac{D_d}{l_{dl}} (\bar{C}_{dl} - \langle C_d \rangle^d) \qquad [43]$$

In recognition of Eq. [42], Eq. [43] can be solved for $\bar{C}_e$ to obtain the following:

$$\bar{C}_e = \frac{\dfrac{\rho_l D_l}{l_{ld}} \langle C_l \rangle^l + \dfrac{\rho_d D_d}{l_{dl}} \langle C_d \rangle^d}{\dfrac{\rho_l D_l}{l_{ld}} + \dfrac{\rho_d D_d}{l_{dl}}} \qquad [44]$$

The use of Eq. [44] to determine $\bar{C}_e$ excludes the possibility of obtaining the envelope velocity, $\bar{w}_{ne}$, from Eq. [43]. Therefore, this velocity is no longer deducible from the conservation equations themselves but must be supplied through an independent relation governing the growth of the dendrite envelope. This is accomplished in Section VI.

VI. GROWTH MODEL FOR THE DENDRITE ENVELOPE

As shown in Figure 1, the envelope is a smooth surface connecting both the primary and secondary dendrite arm tips. Therefore, the envelope velocity, $\bar{w}_{ne}$, can be taken to be equal to some mean tip velocity. Generally, each tip moves at a different speed depending on the local solutal undercooling in the extradendritic liquid adjacent to the tip. In particular, there may be considerable differences in the speeds of the primary and secondary dendrite arm tips. In spite of this complex situation, it is assumed in this study that the mean dendrite tip velocity and, hence, the envelope velocity can be uniquely related to the average solutal undercooling in the extradendritic liquid, *i.e.*, $\bar{C}_e - \langle C_l \rangle^l$. The irregular topography of the envelope caused by the different speeds of the dendrite tips is accounted for through the use of the envelope shape factor as described in Section IV.

Numerous studies have been performed to establish a relation between the dendrite tip undercooling and its growth velocity, and the basic derivations can be found in References 31 and 32. For conciseness, only the final result, written in terms of the present nomenclature, is stated here:

$$\bar{w}_{ne} = \frac{D_l m(\kappa - 1)\bar{C}_e}{\pi^2 \Gamma} [\mathrm{Iv}^{-1}(\Omega)]^2 \qquad [45]$$

where Ω is the dimensionless solutal undercooling and is defined as

$$\Omega = \frac{\bar{C}_e - \langle C_l \rangle^l}{\bar{C}_e(1 - \kappa)} \qquad [46]$$

and $\mathrm{Iv}^{-1}(\Omega)$ is the inverse function of the Ivantsov transport function.[31] Equation [45] assumes a parabolically shaped dendrite tip and neglects the thermal and curvature undercoolings. It is worth noting that Eq. [45] is applicable to both columnar and equiaxed growth, because only solute diffusion is considered. If adopting the hemispherical needle approximation to the shape of a tip, the Ivantsov function simplifies to $\Omega = \mathrm{Iv}(\mathrm{Pe}_t) = \mathrm{Pe}_t$,[31] so that

$$\mathrm{Iv}^{-1}(\Omega) = \Omega \qquad [47]$$

Then, substituting Eq. [47] into Eq. [45], we obtain the following quadratic relation:

$$\bar{w}_{ne} = \frac{D_l m(\kappa - 1)\bar{C}_e}{\pi^2 \Gamma} \Omega^2 \qquad [48]$$

This equation has been used by Rappaz and Thevoz[7] and is employed below in the comparisons for equiaxed solidification.

VII. SUMMARY OF GOVERNING EQUATIONS

A set of model equations is summarized and discussed in this section for situations where the following assumptions can be invoked.

(1) Species diffusion on a macroscopic scale is negligible for all phases (see also Eq. [26]); *i.e.*,

$$D_s^* = D_d^* = D_l^* \approx 0 \qquad [49]$$

(2) The densities of the solid and the liquid phases are equal and constant.

Under these circumstances, the general model presented in the preceding sections reduces to a system of five conservation equations, which can be summarized as follows:

Dendrite envelope motion

$$\frac{\partial}{\partial t}(\varepsilon_s + \varepsilon_d) = S_e \bar{w}_{ne} = \frac{S_e D_l m_l (\kappa - 1)\bar{C}_e}{\pi^2 \Gamma} [\mathrm{Iv}^{-1}(\Omega)]^2 \qquad [50]$$

Solute balance of phase s

$$\frac{\partial(\varepsilon_s \langle C_s \rangle^s)}{\partial t} = \bar{C}_{sd} \frac{\partial \varepsilon_s}{\partial t} + \frac{S_s D_s}{l_{sd}} (\bar{C}_{sd} - \langle C_s \rangle^s) \qquad [51]$$

Solute balance of phase d

$$\frac{\partial(\varepsilon_d \langle C_d \rangle^d)}{\partial t} = (\bar{C}_e - \bar{C}_{ds}) \frac{\partial \varepsilon_s}{\partial t} + \bar{C}_e \frac{\partial \varepsilon_d}{\partial t} + \frac{S_s D_d}{l_{ds}} (\bar{C}_{ds} - \langle C_d \rangle^d) + \frac{S_e D_d}{l_{dl}} (\bar{C}_e - \langle C_d \rangle^d) \qquad [52]$$

Solute balance of phase l

$$\frac{\partial(\varepsilon_l \langle C_l \rangle^l)}{\partial t} = \bar{C}_e \frac{\partial \varepsilon_l}{\partial t} + \frac{S_e D_l}{l_{ld}} (\bar{C}_e - \langle C_l \rangle^l) \qquad [53]$$

Interfacial solute balance at the s-d interface

$$(\bar{C}_{ds} - \bar{C}_{sd}) \frac{\partial \varepsilon_s}{\partial t} = \frac{S_s D_d}{l_{ds}} (\bar{C}_{ds} - \langle C_d \rangle^d) + \frac{S_s D_s}{l_{sd}} (\bar{C}_{sd} - \langle C_s \rangle^s) \qquad [54]$$

Equations [51] through [54] have been obtained by eliminating $\bar{w}_{ns}$ and $\bar{w}_{ne}$ in favor of ε_s and ε_d. They constitute a full system of differential equations for five unknowns: ε_s, ε_d, $\langle C_s \rangle^s$, $\langle C_d \rangle^d$, and $\langle C_l \rangle^l$, while $\bar{C}_e$ is calculated from Eq. [44]. When supplied with the expressions for the diffusion lengths, thermodynamic conditions, and geometrical relations, these equations represent a complete model for solute diffusion. It is noteworthy that all model equations have clear physical interpretations. For example, Eq. [51] simply states that the change in mass of solute in the solid results from the combined contributions of movement of the solid/liquid interface and solute diffusion across the interface. Another salient feature of the present model is that it provides the same set of conservation equations for both equiaxed and columnar dendritic solidification. In other words, the model represents a unified theoretical framework for both modes of solidification while leaving descriptions of the different physical characteristics of each mode to supplementary relations.

VIII. LIMITING CASES

A. *Physical Significance of Limiting Cases*

In this subsection various limiting cases with regard to microscopic solute diffusion in the solid, the interdendritic liquid, and the extradendritic liquid are examined separately. For the solid phase, Eq. [51] indicates two possible limiting cases:

$$\frac{S_s D_s}{l_{sd}} \to \infty \qquad [55]$$

and

$$\frac{S_s D_s}{l_{sd}} = 0 \qquad [56]$$

The first condition implies complete mixing of solute in the solid. Under this circumstance, the volume-averaged concentration, $\langle C_s \rangle^s$, must be equal to the interfacial concentration, $\bar{C}_{sd}$, in order for both sides of Eq. [51] to remain finite. The other limiting case given by Eq. [56] characterizes vanishing solute diffusion in the solid. Recognizing that $S_s \sim 1/\lambda_2$ and $l_{sd} \sim \lambda_2$ (see Eqs. [28] and [A6]), it is apparent that both extremes can be of practical significance. For example, a relatively high solid-mass diffusivity and a small secondary dendrite-arm spacing favor Eq. [55], while a low-mass diffusivity and a relatively large secondary-arm spacing support Eq. [56].

Similarly, Eq. [52] reveals an important limiting case for the interdendritic liquid: the interdendritic liquid becomes solutally well mixed if

$$\frac{S_s D_d}{l_{ds}} \quad \text{or} \quad \frac{S_e D_d}{l_{dl}} \to \infty \qquad [57]$$

Since both sides of Eq. [52] must be finite, Eq. [57] suggests that the average concentration, $\langle C_d \rangle^d$, must be equal to either $\bar{C}_{ds}$ or $\bar{C}_e$. Furthermore, if the microscopic concentration profile in the interdendritic liquid varies monotonically, with the only maxima and minima present at the two interfaces (as shown in Figure 2), Eq. [57] actually implies that the average concentration must be equal to both interfacial concentrations, *i.e.*,

$$\langle C_d \rangle^d = \bar{C}_{ds} = \bar{C}_{dl} = \bar{C}_e \qquad [58]$$

Utilizing the fact that $S_s \sim 1/\lambda_2$ and $l_{ds} \sim \lambda_2$ (see Eq. [A9]), the first condition given by Eq. [57] can equivalently be expressed as

$$\frac{D_d}{\lambda_2^2} \to \infty \qquad [59]$$

For typical liquid-mass diffusivities and secondary-arm spacings occurring in alloy solidification, Eq. [59] is generally satisfied. The assumption of a solutally well-mixed interdendritic liquid is therefore employed throughout the remainder of the article.

Finally, from Eq. [53] we learn that if

$$\frac{S_e D_l}{l_{ld}} \to \infty \qquad [60]$$

a state of complete solutal mixing is reached in the extradendritic liquid. Once more, this condition forces the average liquid concentration to be equal to the corresponding interfacial one in order for both sides of Eq. [53] to remain finite. Physically, Eq. [60] implies that a large envelope area-per-unit volume and a small diffusion length lead to a solutally well-mixed extradendritic liquid.

Note that all terms on the left-hand sides of Eqs. [55] through [57], [59], and [60] represent the inverse of the characteristic time for solute diffusion on the various microscopic scales. Obviously, several combinations of the limiting cases correspond to familiar assumptions that are often utilized in the analysis of alloy solidification. In Section B, the present model equations are simplified for a few selected cases.

B. *Well-Mixed Interdendritic Liquid/Finite-Rate Diffusion in the Extradendritic Liquid*

The first category to be considered assumes finite-rate solute diffusion in the extradendritic liquid and complete diffusion in the interdendritic liquid. Hence, undercooling at the dendrite tips is accounted for in this type of model. Depending on the extent of solute diffusion in the solid, two cases (*i.e.*, finite-rate and vanishing diffusion in the solid) can be further distinguished.

1. *Finite-rate diffusion in the solid*

All model equations can be retained in this case except for Eq. [52], in which the interfacial species fluxes on the right-hand side become indeterminate under Eq. [57]. Their evaluation must resort to the interfacial balances, Eqs. [54] and [43], so that Eq. [52] becomes

$$\varepsilon_d \frac{\partial \bar{C}_e}{\partial t} + (\kappa - 1)\, \bar{C}_e \frac{\partial \varepsilon_s}{\partial t} = -\frac{S_e D_l}{l_{ld}} (\bar{C}_e - \langle C_l \rangle^l) - \frac{S_s D_s}{l_{sd}} (\bar{C}_{sd} - \langle C_s \rangle^s) \quad [61]$$

Now Eqs. [50], [51], [53], and [61] represent the complete set of model equations in this case.

2. *No diffusion in the solid*

By neglecting solute diffusion in the solid, as stated by Eq. [56], all terms involving D_s on the right-hand sides of Eqs. [51] and [61] vanish, so that the equations simplify to

$$\frac{\partial (\varepsilon_s \langle C_s \rangle^s)}{\partial t} = \kappa \bar{C}_e \frac{\partial \varepsilon_s}{\partial t} \quad [62]$$

$$\varepsilon_d \frac{\partial \bar{C}_e}{\partial t} + (\kappa - 1) \bar{C}_e \frac{\partial \varepsilon_s}{\partial t} = -\frac{S_e D_l}{l_{ld}} (\bar{C}_e - \langle C_l \rangle^l) \quad [63]$$

where use has been made of the fact that $\bar{C}_{sd} = \kappa \bar{C}_e$ and $\bar{C}_{ld} = \bar{C}_e$, in order to reduce the number of unknowns. Also, for reasons that will become apparent subsequently, we rewrite Eq. [53] as

$$\varepsilon_l \frac{\partial \langle C_l \rangle^l}{\partial t} = \left(\frac{S_e D_l}{l_{ld}} + \frac{\partial \varepsilon_l}{\partial t} \right) (\bar{C}_e - \langle C_l \rangle^l) \quad [64]$$

Now, Eqs. [50] and [62] through [64] represent a complete model for both equiaxed and columnar dendritic solidification in cases where the assumptions of a well-mixed interdendritic liquid and vanishing solute diffusion in the solid can be invoked. It is noteworthy that Eq. [62] is uncoupled from the other differential equations and only needs to be solved if $\langle C_s \rangle^s$ is desired.

There is another interesting observation that follows from Eq. [64]: to be physically meaningful, $d\langle C_l \rangle^l / dt$ must be greater than zero, which leads to the following:

$$l_{ld} \leq -\frac{S_e D_l}{d\varepsilon_l / dt} = \frac{D_l}{\bar{w}_{ne}} \quad [65]$$

This poses a constraint on the diffusion length. The expressions for the length l_{ld} developed in the Appendix satisfy this constraint and are therefore suitable for incorporation in the present model.

C. *Well-Mixed Interdendritic and Extradendritic Liquids*

In order to investigate this more restricted case, it is instructive to write down the overall solute balance that results from summing up the species conservation equations for all three phases and canceling out the interfacial terms; namely,

$$\frac{\partial}{\partial t} (\varepsilon_l \langle C_l \rangle^l) + \frac{\partial}{\partial t} (\varepsilon_d \langle C_d \rangle^d) + \frac{\partial}{\partial t} (\varepsilon_s \langle C_s \rangle^s) = 0 \quad [66]$$

For solutally well-mixed l and d phases, Eq. [66] can be simplified as

$$\frac{\partial}{\partial t} [(1 - \varepsilon_s) \bar{C}_e] + \frac{\partial}{\partial t} (\varepsilon_s \langle C_s \rangle^s) = 0 \quad [67]$$

or, in integrated form,

$$(1 - \varepsilon_s) \bar{C}_e + \varepsilon_s \langle C_s \rangle^s = C_0 \quad [68]$$

Now, depending on the extent of solute diffusion in the solid, the following three subcases result.

(1) Complete diffusion in the solid

In this case, we have that $\langle C_s \rangle^s = \bar{C}_{sd} = \kappa \bar{C}_e$, and Eq. [67] reduces to the following differential form of the Lever rule:

$$d\bar{C}_e - d[\varepsilon_s (1 - \kappa) \bar{C}_e] = 0 \quad [69]$$

(2) No diffusion in the solid

Making use of Eq. [62], Eq. [67] leads to the following differential form of Scheil's equation:

$$d[(1 - \varepsilon_s) \bar{C}_e] + \kappa \bar{C}_e d\varepsilon_s = 0 \quad [70]$$

(3) Finite-rate diffusion in the solid

In this case, the present model reduces to a set of only two equations, namely, Eqs. [51] and [67]. Restricting further attention to a parabolic solidification rate, Eq. [51] can be rewritten as

$$\varepsilon_s \frac{d\langle C_s \rangle^s}{d\varepsilon_s} = (1 + 6\alpha) (\kappa \bar{C}_e - \langle C_s \rangle^s) \quad [71]$$

where the independent variable has been changed from t to ε_s with the help of the parabolic solidification equation $\varepsilon_s d\varepsilon_s / dt = 1/2t_f$. Use has also been made of the

relations $S_s = 2/\lambda_2$ and $l_{sd} = \varepsilon_s\lambda_2/6$ as developed previously. The parameter α is the traditional diffusion Fourier number based on the secondary dendrite-arm spacing, which characterizes the extent of solute diffusion in the solid. Further substituting $\bar{C}_e$ for $\langle C_s\rangle^s$ in recognition of Eq. [68], one arrives at the following first-order differential equation for $\bar{C}_e$:

$$\frac{d\bar{C}_e}{d\varepsilon_s} + \left[\frac{(1 + 6\alpha)\kappa - 1}{1 - \varepsilon_s} + \frac{6\alpha}{\varepsilon_s}\right]\bar{C}_e = \frac{6\alpha}{\varepsilon_s(1 - \varepsilon_s)}C_0 \qquad [72]$$

which has a closed-form analytical solution for finite and constant values of α:

$$\frac{\bar{C}_e}{C_0} = \frac{6\alpha(1 - \varepsilon_s)^{(1+6\alpha)\kappa-1}}{\varepsilon_s^{6\alpha}}\int_0^{\varepsilon_s}\varepsilon^{6\alpha-1}(1 - \varepsilon)^{-(1+6\alpha)\kappa}d\varepsilon \qquad [73]$$

It has been shown[33] that Eq. [73] produces accurate results for microsegregation of P in δ-Fe. To obtain a more simple expression for microsegregation, Ohnaka[34] introduced additional assumptions in his integral method.

IX. ILLUSTRATIVE EXAMPLES

Illustrative calculations are carried out in order to compare the present multiphase model to several previous models for dendritic solidification. For the sake of clarity, comparisons are made separately for purely equiaxed, purely columnar, and, finally, mixed columnar-equiaxed solidification.

A. *Equiaxed Growth*

Two solute diffusion models for equiaxed dendritic growth have been put forward by Rappaz and Thevoz.[7,8] In both models, it is assumed that there is absent back diffusion in the solid and complete mixing of solute in the interdendritic liquid. Therefore, the simplified version of the multiphase model, consisting of Eqs. [50] and [62] through [64], is a suitable candidate for direct comparison with the two studies. Also, Rappaz and Thevoz[7,8] assume a spherical dendrite envelope, so that the shape factor in Eq. [35] should be taken equal to unity. It can be seen that the present multiphase model differs from that of Rappaz and Thevoz[7] only in that the former model utilizes an integral representation of solute diffusion in the extradendritic liquid together with the concept of a diffusion length, while Rappaz and Thevoz[7] solve a partial differential equation instead. However, this difference would not be of significant consequence, because the present diffusion length is derived from an analytical solution of the differential equation governing solute diffusion in the extradendritic liquid (Appendix).

The second model of Rappaz and Thevoz[8] is analytical in nature and can thus be compared more closely. If it is assumed in the present model that the average concentration, $\langle C_l\rangle^l$, outside the envelope remains equal to its initial value, C_0, such that $d\langle C_l\rangle^l/dt = 0$, then the species conservation equation, Eq. [64], reduces to

$$l_{ld} = \frac{D_l}{\bar{w}_{ne}} \qquad [74]$$

This is exactly the key result in the analytical model of Rappaz and Thevoz.[8] However, Eq. [74] should not be deemed as another general expression for the liquid diffusion length (compare to Eq. [A18]), because the assumption on which Eq. [74] is based may not generally be valid. Moreover, this assumption leads to the failure of arriving at a state of complete solute mixing in the liquid during the later stages of solidification. As a remedy, Rappaz and Thevoz[8] implement a certain correction procedure so as to ensure a smooth transition to the state of complete solute mixing. By contrast, the use of Eq. [A18] together with the solute conservation equation for the extradendritic liquid, Eq. [64], does not suffer from these shortcomings.

To illustrate these comparisons quantitatively, a numerical study based on the present model has been performed for a uniformly solidifying system with an equiaxed dendritic morphology. The system is chosen to be the same as that studied by Rappaz and Thevoz.[7] The temperature is assumed to be uniform, so that the energy equation can be written as:[7]

$$c_p\dot{T} = \Delta h\frac{d\varepsilon_s}{dt} - c_p m_l\frac{d\bar{C}_e}{dt} \qquad [75]$$

Also, the quadratic relation, Eq. [48], is employed as the growth model for the dendrite tips (*i.e.*, $\mathrm{Iv}^{-1}(\Omega) = \Omega$ in Eq. [50]). The initial conditions for Eqs. [50], [62] through [64], and [75] are $\varepsilon_s = \varepsilon_d = 0$, $\langle C_s\rangle^s = \kappa C_0$, and $\bar{C}_e = \langle C_l\rangle^l = C_0$. This set of equations is numerically solved using the standard fourth-order Runge-Kutta method. Results are obtained for an Al-5 wt pct Si alloy, a cooling rate, $\dot{T}$, of 45 K s^{-1}, and three different nuclei densities: $n = 2.39 \times 10^{11}$, 2.39×10^{8}, and 2.39×10^{5} m^{-3}, which correspond to final grain radii of 10^{-4}, 10^{-3}, and 10^{-2} m, respectively. It is assumed that nucleation occurs instantaneously at the liquidus temperature. The physical properties are taken from Reference 7.

The predicted cooling curves near the recalescence stage are displayed in Figure 4, where the more exact solutions due to Rappaz and Thevoz[7] are shown as dashed lines. It is seen that the two predictions are indeed in close agreement, as they should. The minor difference for the case of $n = 2.39 \times 10^{11}$ m^{-3} is due to the fact that the present model utilizes an approximate analytical diffusion length, while Rappaz and Thevoz's model[7] calculates solute diffusion in the extradendritic liquid more accurately from a partial differential equation. However, a comprehensive parametric study using different choices of the diffusion length leads to the conclusion that the diffusion length is not a crucial factor in the present model.[33] This, by the way, explains why the second model of Rappaz and Thevoz[8] employing the approximate diffusion length, Eq. [74], yields good results.

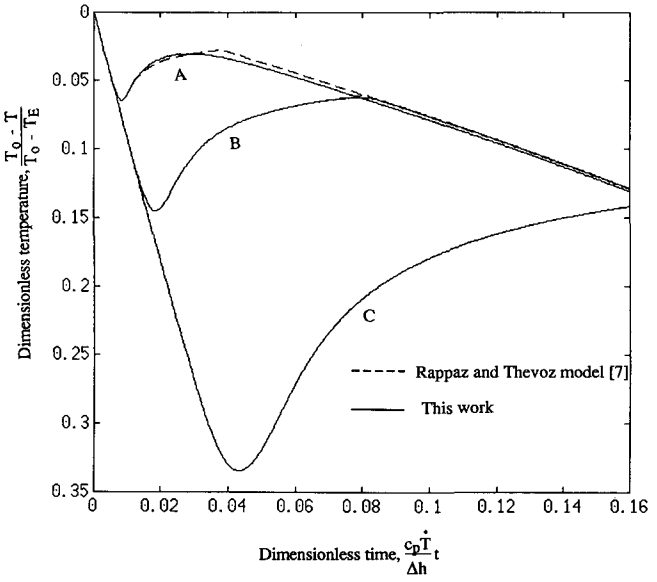

Fig. 4—Comparison of cooling curves for equiaxed solidification of an Al-5 wt pct Si alloy and nuclei density of (*a*) 2.39 × 10^{11} m^{-3}, (*b*) 2.39 × 10^{8} m^{-3}, and (*c*) 2.39 × 10^{5} m^{-3}.

B. *Columnar Solidification*

For columnar dendritic solidification, we employ the same assumptions as in the equiaxed case, which include no macroscopic species diffusion, equal densities of the solid and liquid phases, no solute diffusion in the solid, and complete mixing of solute in the interdendritic liquid. Hence, the simplified model given by Eqs. [50] and [61] through [64] is still applicable in the present situation.

There have been several attempts to incorporate dendrite-tip undercooling into microsegregation models for columnar growth. Flood and Hunt[9] and, more recently, Kerr *et al.*[11] simply truncate the Scheil equation at the tip temperature. However, this model fails to satisfy the solute balance, as pointed out by Rappaz.[2] This can be illustrated using the present model, as explained subsequently.

Summing up Eqs. [63] and [64] yields the following conservation equation (note that $\bar{C}_e$ is equal to the liquid concentration at the solid/liquid interface; see Eq. [58]):

$$(1 - \varepsilon_s)\frac{d\bar{C}_e}{dt} + (\kappa - 1)\,\bar{C}_e\frac{d\varepsilon_s}{dt} = \frac{d}{dt}[\varepsilon_l(\bar{C}_e - \langle C_l\rangle^l)] \quad [76]$$

where the interfacial terms have canceled out. By arranging the left-hand side in the differential form of Scheil's equation, it becomes clear that the two previous studies[9,11] neglected the tip undercooling in the solute conservation equation; *i.e.*,

$$\bar{C}_e - \langle C_l\rangle^l \approx 0 \quad [77]$$

With this simplification the right-hand side of Eq. [76] vanishes and the left-hand side can be integrated to yield Scheil's equation:

$$\varepsilon_s = 1 - \left(\frac{C_0}{\bar{C}_e}\right)^{1/(1-\kappa)} \quad [78]$$

which was used to calculate the solid volume fraction. Obviously, Eq. [78] is not solute conserving in the presence of tip undercooling.

The other more recent model of columnar solidification by Giovanola and Kurz[10] is free from the preceding shortcoming and conserves solute everywhere. The model treats the mushy zone as two regions, with undercooling accounted for only in the tip region and a state of complete solute mixing assumed in the region where the solid fraction exceeds a sufficiently large value. Then, an empirical curve fit is applied to construct the solid fraction profile in the tip region, and Scheil's equation is utilized in the other region. In contrast, the present model employs a single differential equation that is valid throughout the mushy region; *i.e.*,

$$(1 - \varepsilon_s)\frac{d\bar{C}_e}{d\varepsilon_s} + (\kappa - 1)\bar{C}_e = \frac{d}{d\varepsilon_s}[\varepsilon_l(\bar{C}_e - \langle C_l\rangle^l)] \quad [79]$$

Equation [79] is obtained by rewriting Eq. [76] in terms of ε_s. With increasing ε_s (*i.e.*, away from the tip region), the undercooling diminishes in the extradendritic liquid and gradually approaches zero (so does the liquid fraction). As a result, Eq. [79] naturally reduces to Scheil's equation in an asymptotic manner.

For a volume element containing columnar dendrites whose temperature is nearly uniform, it is reasonable to assume a constant cooling rate, namely

$$-\frac{dT}{dt} = -m_l\frac{d\bar{C}_e}{dt} = \dot{T} \quad [80]$$

where the cooling rate is equal to the product of the growth velocity of the columnar front, V_t, and the thermal gradient. The latter can be determined by, for example, the heat flow model of Campagna.[35,36] The appropriate initial conditions to Eqs. [50], [62] through [64], and [80] are $\varepsilon_s = \varepsilon_d = 0$, $\langle C_l\rangle^l = C_0$, and $\bar{C}_e - C_0 = f(V_t)$, respectively, with the last relation obtained from the growth model, Eq. [45]. Solving this set of equations simultaneously, a microsegregation pattern in the presence of tip undercooling can be predicted. An example calculation has been performed for an Ag-15 wt pct Cu alloy with the front velocity equal to 0.12 m s^{-1} and a primary arm spacing of 0.3 μm.[37] The interface kinetics are accounted for by using a kinetic instead of equilibrium partition coefficient, as done in Giovanola and Kurz.[10] The physical properties of the alloy have been listed in Wang and Beckermann.[33] The predicted microsegregation pattern is presented in Figure 5. It is seen that for this case of rapid solidification, the microsegregation curve greatly deviates from the described by the Scheil equation, and solidification proceeds at an almost constant concentration until a state of complete solutal mixing in the liquid is reached. In addition, three important features may be noted from Figure 5. In comparison to the Scheil model: (1) the concentration in the initially solidified solid is higher, (2) the concentration in the finally formed solid is lower, and (3) the eutectic fraction decreases. Also shown in Figure 5 are Giovanola and Kurz's predictions[10] and experimental data of Bendersky and Boettinger.[37] It is observed that the present prediction agrees well with

Giovanola and Kurz's result as well as with the experimental data.

C. *Mixed Columnar-Equiaxed Solidification*

With the allowance of undercooling at the columnar front and in the presence of nucleation sites in the bulk liquid, equiaxed grains can appear and subsequently grow ahead of the advancing columnar front. This results in a mixed columnar-equiaxed growth structure in a casting. At present, there are few models available for this mixed type of solidification and the prediction of the columnar-to-equiaxed transition (CET) in solidified alloys. The only attempt by Flood and Hunt[9] utilizes the truncated Scheil equation as discussed in Section B.

Since the present model features a set of conservation equations that is applicable to both modes of solidification, a single-domain, fixed-grid numerical methodology for mixed columnar-equiaxed solidification becomes possible. The columnar front is tracked only for the purpose of specifying the complementary relations in the different subregions having different dendrite morphologies. This can be done using the implicit scheme recently developed by the present authors.[38] The finite-volume method[39] is employed to solve the heat equation,[2] and the present solute-diffusion model is integrated by simple time-marching. A two time-step technique is introduced to allow for a much smaller time-step in the solution of the solute-diffusion model, while keeping a reasonably large time-step in solving the heat-flow equation. The reader is referred to Wang and Beckermann[38] for more details on the numerical technique used in the CET simulations. The CET position is considered to occur when the equiaxed grain-volume fraction ($1 - \varepsilon_l = \varepsilon_s + \varepsilon_d$) immediately ahead of the columnar front is equal to 0.49, a criterion developed by an argument regarding the probability of a columnar trunk being obstructed by sufficiently large equiaxed grains.[40]

One-dimensional simulations have been carried out to simulate a series of experimental runs conducted by Ziv and Weinberg[41] for an Al-3 wt pct Cu alloy in a 100-mm-wide mold, using the physical properties of the alloy listed in.[38] The mold bottom is subject to a convective cooling condition so that solidification proceeds vertically upward. Some preliminary numerical results for the CET as a function of the convective heat transfer coefficient are displayed in Figure 6 together with the experimental data of Ziv and Weinberg.[41] The grid size of the computational mesh for the results presented here was 2.5 mm, and the time-step was 0.05 second during the nucleation period and 0.5 second after the termination of nucleation. It can be seen that the prediction of the CET position is in qualitative agreement with the experiments. More detailed comparisons between theory and experiment can be found in Wang and Beckermann.[38]

X. CONCLUSIONS

A multiphase approach to the modeling of solute diffusion during dendritic alloy solidification is proposed. The macroscopic transport equations are developed separately for the solid phase, the interdendritic liquid, and the extradendritic liquid, using the technique of volume averaging. The model distinguishes different microscopic length scales present in a dendritic structure and

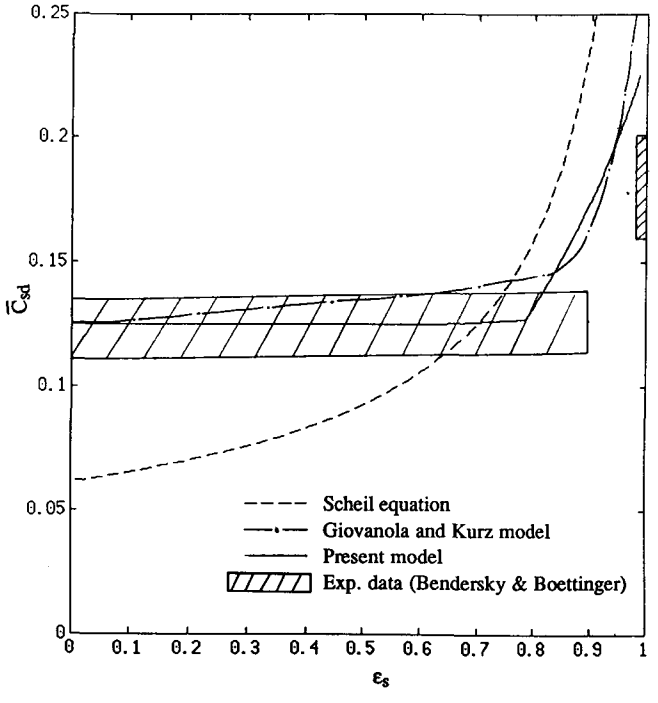

Fig. 5—Comparison of microsegregation profiles for a Ag-15 wt pct Cu alloy solidified with a columnar dendrite tip velocity of 0.12 m s^{-1}. The crosshatched regions are the range of experimental data measured by Bendersky and Boettinger.[37]

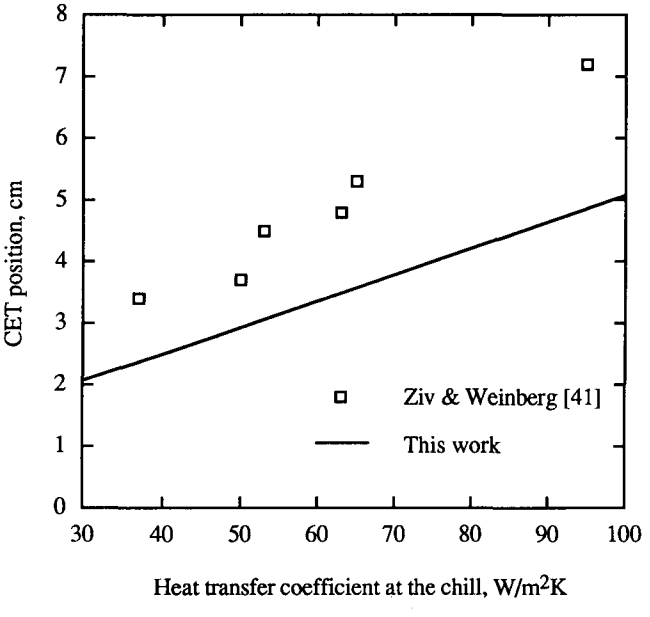

Fig. 6—Comparison of predicted CET with experimental data of Ziv and Weinberg[41] for a one-dimensional Al-3 wt pct Cu casting. The calculations employ the growth model for a parabolic tip, Eq. [45], and a modified instantaneous nucleation law[42] that results in an exact match with the measured grain density in the equiaxed zone: $n = K_3 + K_4(dT/dt)^2$, with $K_3 = 10^6$ m^{-3} and $K_4 = 10^{10}$ s^2 K^{-2} m^{-3}.

links the microscopic phenomena occurring on each length scale to the macroscopic equations. In particular, the model incorporates dendrite tip growth in the presence of undercooling in the extradendritic liquid, as well as accounts for dendrite geometry, coarsening, and finite-rate solute diffusion in the solid. The model should lead to improved predictions of dendritic solidification and microstructure formation on the system scale. Furthermore, the present model consists of a single set of conservation equations for both equiaxed and columnar growth, thus providing a unified theoretical framework for both modes of solidification. Illustrative calculations have shown that the proposed model is successful in addressing a variety of phenomena, such as recalescence in equiaxed growth, dendrite tip undercooling during rapid columnar solidification, and CET.

Efforts are currently underway to generalize the model to include melt convection and solid movement (for equiaxed grains) utilizing the same multiphase approach.

NOMENCLATURE

a	constant, in the Appendix
A	interfacial area, m^2
A_s	area of the solid/interdendritic liquid interface, m^2
A_e	area of the dendrite envelope, m^2
b	constant, in the Appendix
c	constant, in the Appendix
C	concentration of a chemical species, weight percent
c_p	volumetric specific heat, J m^{-3} K^{-1}
d	microscopic length scale, m
d_s	mean characteristic length or diameter of the solid phase, m
d_e	mean characteristic diameter of the dendrite envelope, m
D	diffusion coefficient, m^2 s^{-1}
Iv	Ivantsov function
$\mathbf{j}$	species diffusion flux, kg m^{-2} s^{-1}
J	interfacial species transfer rate per unit of volume, kg m^{-3} s^{-1}
k	constants in the nucleation law, see Figure 6
l	species diffusion length, m
L	macroscopic length scale, m
m_l	liquidus line slope
n	nuclei density, m^{-3}
$\mathbf{n}$	outwardly directed unit normal vector
Pe	envelope Peclet number, $\bar{\mathbf{w}}_{ne}R_f/D_l$
Pe_t	solutal Peclet number at the dendrite tip, $V_tR_t/2D_l$
r	radial coordinate
R	radius, m
S	interfacial area concentration, A_k/V_0, m^{-1}
S_v	specific interfacial area, A_k/V_k, m^{-1}
t	time, s
T	temperature, K
$\dot{T}$	cooling rate, K s^{-1}
v	velocity, m s^{-1}
V_k	volume of phase k, m^3
V_0	averaging volume, m^3
V_t	dendrite tip velocity, m s^{-1}
$\mathbf{w}$	interface velocity, m s^{-1}
w_n	normal interface velocity, ms^{-1}
$\mathbf{x}$	position vector
X	phase function

Greek Symbols

α	diffusion Fourier number, $4D_st_f/\lambda_2^2$
β	a factor
Γ	interfacial mass transfer rate due to interface movement (kg m^{-3} s^{-1}) or Gibbs-Thomson coefficient (mK)
Δh	volumetric latent heat of phase change, J m^{-3}
ε	volume fraction
κ	partition coefficient
λ	dendrite arm spacing, m
ρ	density, kg m^{-3}
ϕ	shape factor
Φ	a field property
Ψ	a field property
Ω	solutal supersaturation

Subscripts

d	interdendritic liquid
e	dendrite envelope
f	final dimension of the dendrite envelope
j	phase j
k	phase k
kj	pertinent to phase k on the k-j interface
l	extradendritic liquid
m	melting point of pure metal
n	normal direction
o	initial state
r	in the r-direction
s	solid
t	dendrite tip

Superscripts

j	due to species gradients
Γ	due to interface movement
$\bar{}$	interfacial area—averaged
$*$	effective or dimensionless

APPENDIX

Microscopic analysis of the diffusion lengths

Solid region

The modeling of the diffusion length in the solid is important for the prediction of finite-rate solute diffusion and, hence, microsegregation in a solidified alloy. For dendritic solidification, Ohnaka[34] has presented an elegant model that gives good agreement with experimental data and fits well into the framework of the present formulation. Following his procedure, the present derivation is based on a one-dimensional platelike dendrite arm geometry, as shown in Figure A1. A parabolic concentration distribution is assumed in the solid

$$C_s = a + bx + cx^2 \qquad [A1]$$

The three coefficients are determined by the following boundary conditions

$$\frac{dC_s}{dx} = 0 \quad \text{at} \quad x = 0 \text{ (symmetry)} \qquad [A2]$$

$$C_s = \bar{C}_{sd} \quad \text{at} \quad x = d_s/2 \qquad [A3]$$

and the known volume-averaged concentration, $\langle C_s \rangle^s$, which can be calculated from

$$\langle C_s \rangle^s = \frac{2}{d_s} \int_0^{d_s/2} C_s dx \qquad [A4]$$

Using Eqs. [A2], [A3], and [A4], the concentration profile is found to be given by

$$\frac{\bar{C}_{sd} - C_s}{\bar{C}_{sd} - \langle C_s \rangle^s} = \frac{6}{d_s} (d_s^2/4 - x^2) \qquad [A5]$$

With the definition of the diffusion length, Eq. [23], it is readily shown that

$$l_{sd} = d_s/6 \qquad [A6]$$

The mean diameter of the solid phase, d_s, can be related to the secondary dendrite arm spacing, λ_2, and the volume fraction ε_s (Section IV). The derivation can be modified for other dendrite arm geometries such as cylinders and spheres. The same result is obtained except for a change in the numerical factor of the order of unity.

Interdendritic liquid

For a dendrite envelope closely encompassing the dendrite arms, a similar analysis as that for the solid yields that the diffusion lengths in the interdendritic liquid, l_{ds} and l_{dl}, are proportional to the characteristic interdendritic spacing; *i.e.*,

$$l_{ds} = \beta_1 \frac{(\lambda_2 - d_s)}{2} \qquad [A7]$$

$$l_{dl} = \beta_2 \frac{(\lambda_2 - d_s)}{2} \qquad [A8]$$

where β_1 and β_2 are constants of the order of unity. In recognition of Eq. [27], the two diffusion lengths given by Eqs. [A7] and [A8] suggest that

$$l_{ds} \quad \text{and} \quad l_{dl} \sim \lambda_2 \qquad [A9]$$

Together with Eq. [A6], this implies that diffusion lengths in the interdendritic liquid and the solid are of the same order of magnitude. However, because the liquid mass diffusivity is typically several orders of magnitude larger than that of the solid, it is usually safe to assume that the interdendritic liquid is solutally well mixed and, thus, it is unimportant to accurately model finite-rate solute diffusion in the interdendritic liquid.

Extradendritic liquid

In contrast, one has to carefully model the diffusion length in the liquid outside the dendrite envelope in order to account for solutal undercooling of the liquid ahead of the dendrite tips. This is done here by assuming that: (1) the envelope is spherical with an equivalent radius R_e and (2) solute diffusion is quasi-steady in the moving coordinate system fixed to the envelope surface, as illustrated in Figure A2.

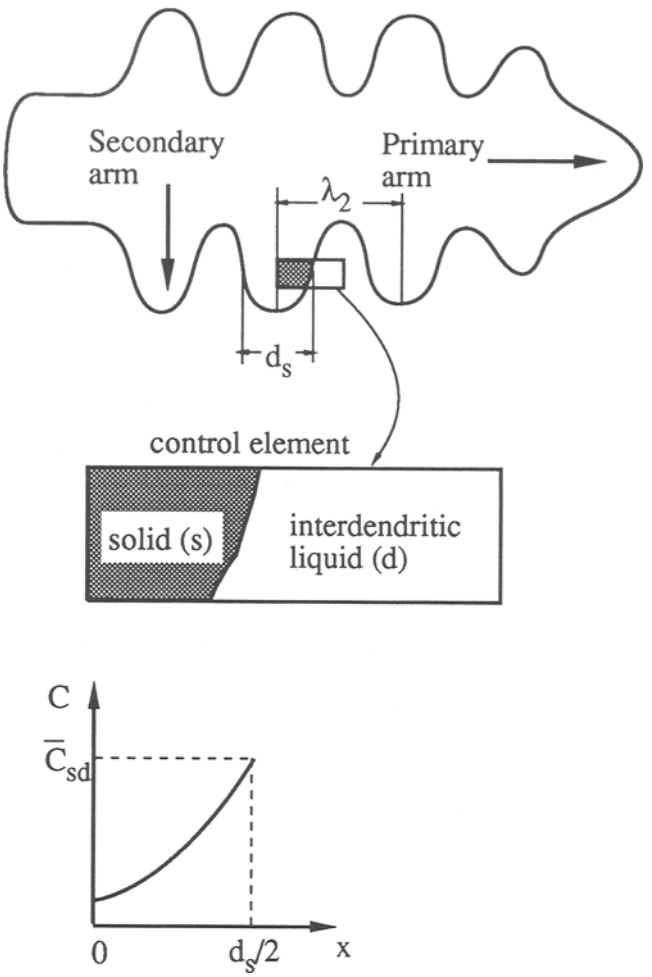

Fig. A1 — One-dimensional, platelike model of a dendrite arm and illustration of the solid concentration profile.

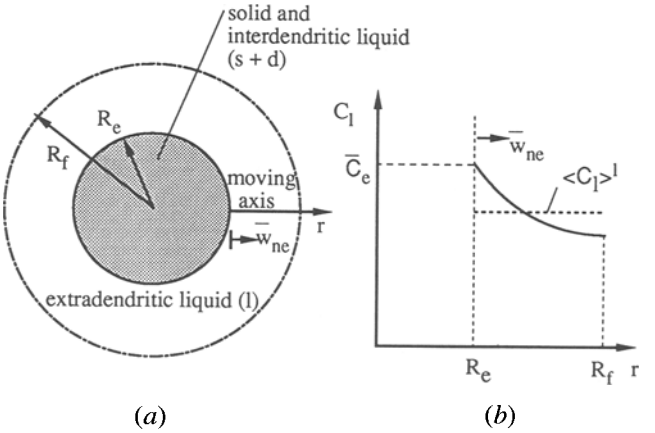

Fig. A2 — Equivalent sphere model for species diffusion in the extradendritic liquid: (*a*) geometry and (*b*) concentration profile.

The differential equation governing solute diffusion in the interdendritic liquid can now be written as

$$v_r \frac{dC_l}{dr} = \frac{D_l}{r^2} \frac{d}{dr}\left(r^2 \frac{dC_l}{dr}\right) \qquad [A10]$$

The liquid around the envelope moves relative to the moving coordinate system at a radial velocity whose distribution is obtained from the continuity equation as

$$v_r = -\bar{w}_{ne}\left(\frac{R_e}{r}\right)^2 \qquad [A11]$$

Equation [A10], together with the velocity profile given by Eq. [A11], admits a general solution of the form of

$$C_l = a + b \exp\left(\bar{w}_{ne} R_e^2 / D_l r\right) \qquad [A12]$$

By introducing a Peclet number that is based on the final equivalent radius, R_f, of the dendrite envelope

$$\mathrm{Pe} = \frac{\bar{w}_{ne} R_f}{D_l} \qquad [A13]$$

and a dimensionless radius

$$r^* = r/R_f \qquad [A14]$$

Equation [A12] is recast into

$$C_l = a + b \exp\left[\frac{\mathrm{Pe}}{r^*}(1 - \varepsilon_l)^{2/3}\right] \qquad [A15]$$

where use has been made of the fact that $R_e/R_f = (1 - \varepsilon_l)^{1/3}$. The constants a and b are determined by the following conditions

$$C_l = \bar{C}_{ld}, \quad \text{at} \quad r^* = r_e^* = (1 - \varepsilon_l)^{1/3} \qquad [A16]$$

$$\langle C_l \rangle^l = \frac{1}{V_l}\int_{V_l} C_l dV = \frac{3}{\varepsilon_l}\int_{(1-\varepsilon_l)^{1/3}}^{1} r^{*2} C_l dr^* \qquad [A17]$$

With the concentration profile found, substitution into the definition of the diffusion length yields

$$l_{ld}/R_f = \frac{1}{\mathrm{Pe}}\left(1 - \frac{3}{\varepsilon_l}\exp\left[-\mathrm{Pe}(1 - \varepsilon_l)^{1/3}\right] \cdot \int_{(1-\varepsilon_l)^{1/3}}^{1} x^2 \exp\left[\frac{\mathrm{Pe}(1 - \varepsilon_l)^{2/3}}{x}\right] dx\right) \qquad [A18]$$

where x is a dummy variable of integration. The integral requires numerical evaluation.

This derivation for the liquid diffusion length can also be performed for cylindrical and Cartesian coordinate systems. Due to length limitations, only the final results are presented here:

$$l_{ld}/R_f = \frac{1}{\mathrm{Pe}}\left(1 - \frac{2}{\varepsilon_l}\exp\left[\frac{\mathrm{Pe}}{2}(1 - \varepsilon_l)^{1/2}\ln(1 - \varepsilon_l)\right] \cdot \int_{(1-\varepsilon_l)^{1/2}}^{1} x \exp\left[-\mathrm{Pe}(1 - \varepsilon_l)^{1/2}\ln x\right] dx\right) \qquad [A19]$$

for a cylindrical envelope and

$$l_{ld}/R_f = \frac{1}{\mathrm{Pe}}\left(1 - \frac{1}{\varepsilon_l \mathrm{Pe}}\left[1 - \exp\left(\varepsilon_l \mathrm{Pe}\right)\right]\right) \qquad [A20]$$

for a platelike envelope. Equation [A18] is useful for equiaxed growth, while Eq. [A19] is applicable to the columnar case.

Last, it is worth noting that the diffusion lengths given by Eqs. [A18], [A19], and [A20] all share the property that

$$l_{ld}/R_f \leq \frac{1}{\mathrm{Pe}} \qquad [A21]$$

or alternatively,

$$l_{ld} \leq \frac{D_l}{\bar{w}_{ne}} \qquad [A22]$$

ACKNOWLEDGMENTS

This work was supported by the National Science Foundation under Grant No. CTS-8957149 and by the ALCOA Technical Center, Alcoa Center, PA.

REFERENCES

1. C. Beckermann and R. Viskanta: *Appl. Mech. Rev.*, 1993, vol. 46, pp. 1-27.
2. M. Rappaz: *Int. Mater. Rev.*, 1989, vol. 34, pp. 93-123.
3. V.R. Voller, M.S. Stachowicz, and B.G. Thomas: *Materials Processing in the Computer Age*, TMS, Warrendale, PA, 1991.
4. J. Ni and C. Beckermann: *Metall. Trans. B*, 1991, vol. 22B, pp. 349-61.
5. S. Ganesan and D.R. Poirier: *Metall. Trans. B*, 1990, vol. 21B, pp. 173-81.
6. I. Dustin and W. Kurz: *Z. Metallkd.*, 1986, vol. 77, pp. 265-73.
7. M. Rappaz and Ph. Thevoz: *Acta Metall.*, 1987, vol. 35, pp. 1487-97.
8. M. Rappaz and Ph. Thevoz: *Acta Metall.*, 1987, vol. 35, pp. 2929-33.
9. S.C. Flood and J.D. Hunt: *Appl. Sci. Res.*, 1987, vol. 44, pp. 27-42.
10. B. Giovanola and W. Kurz: *Metall Trans. A*, 1990, vol. 21A, pp. 260-63.
11. R.C. Kerr, A.W. Woods, M.G. Worster, and H.E. Huppert: *J. Fluid Mech.*, 1990, vol. 217, pp. 331-48.
12. N. Wakao and J.M. Smith: *Chem. Eng. Sci.*, 1962, vol. 17, pp. 825-34.
13. O.A. Plumb and S. Whitaker: in *Dynamics of Fluids in Hierarchical Porous Media*, J.H. Cushman, ed., Academic Press, London, 1990, pp. 97-148.
14. M. Kaviany: *Principles of Heat Transfer in Porous Media*, Springer-Verlag, New York, NY, 1991.
15. C.Y. Wang and C. Beckermann: *Int. J. Multiphase Flow*, 1993, vol. 19, pp. 397-407.
16. D.A. Drew: *Annu. Rev. Fluid Mech.*, 1983, vol. 15, pp. 261-91.

17. S.M. Hassanizadeh and W.G. Gray: *Adv. Water Resour.*, 1979, vol. 2, pp. 131-44.
18. S.M. Hassanizadeh and W.G. Gray: *Adv. Water Resour.*, 1979, vol. 2, pp. 191-208.
19. S.M. Hassanizadeh and W.G. Gray: *Adv. Water Resour.*, 1980, vol. 3, pp. 25-41.
20. M. Rappaz and V.R. Voller: *Metall. Trans. A*, 1990, vol. 21A, pp. 749-53.
21. D.R. Poirier, P.J. Nandapurkar, and S. Ganesan: *Metall. Trans. B*, 1991, vol. 22B, pp. 889-900.
22. S.P. Marsh and M.E. Glicksman: in *Modeling of Casting, Welding and Advanced Solidification Processes VI*, T.S. Piwonka, V. Voller, and L. Katgerman, eds., TMS, Warrendale, PA, 1993, pp. 55-62.
23. M.E. Glicksman, R.N. Smith, S.P. Marsh, and R. Kuklinski: *Metall. Trans. A*, 1992, vol. 23A, pp. 659-67.
24. R.T. DeHoff and F.N. Rhines: *Quantitative Microscopy*, McGraw-Hill, New York, NY, 1968.
25. R.B. Bird, W.E. Stewart, and E.N. Lightfoot: *Transport Phenomena*, John Wiley, New York, NY, 1960, p. 167.
26. T.Z. Kattamis, J.C. Coughlin, and M.C. Flemings: *Trans. TMS-AIME*, 1967, vol. 239, pp. 1504-11.
27. S.P. Marsh, M.E. Glicksman, L. Meloro, and K. Tsutsumi: in *Modeling and Control of Casting and Welding Processes IV*, A.F. Giame and G.J. Abbashian, eds., TMS, Warrendale, PA, 1988, pp. 15-23.
28. M. Avrami: *J. Chem. Phys.*, 1940, vol. 8, pp. 212-24.
29. G.R. Speich and R.M. Fisher: in *Recrystallization, Grain Growth and Textures*, Margolin, H., ed., ASM, Metals Park, OH, 1966, pp. 563-98.
30. S. Ahuja, C. Beckermann, R. Zakhem, P.D. Weidman, and H.C. deGroh III: in *Micro/Macro Scale Phenomena in Solidification*, C. Beckermann, L.A. Bertram, S.J. Pien, and R.E. Smelser, eds., ASME, New York, NY, 1992, pp. 85-91.
31. W. Kurz and D.J. Fisher: *Fundamentals of Solidification*, Trans. Tech Publications, Aedermannsdorf, Switzerland, 1989.
32. J. Lipton, M.E. Glicksman, and W. Kurz: *Mater. Sci. Eng.*, 1984, vol. 65, pp. 57-63.
33. C.Y. Wang and C. Beckermann: *Mat. Sci. Eng. A*, 1993, in press.
34. I. Ohnaka: *Trans. Iron Steel Inst. Jpn.*, 1986, vol. 26, pp. 1045-51.
35. A.J. Campagna: Ph.D. Thesis, Massachusetts Institute of Technology, Cambridge, MA, 1970.
36. M.C. Flemings: *Metall. Trans. A*, 1991, vol. 22A, pp. 957-81.
37. L.A. Bendersky and W.J. Boettinger: in *Rapidly Quenched Metals*, S.S. Warlimont, ed., 1985, vol. 1, pp. 887-90.
38. C.Y. Wang and C. Beckermann: *Metall. Trans. A*, 1993, vol. 24A, in press.
39. S.V. Patankar: *Numerical Heat Transfer and Fluid Flow*, Hemisphere Publishing Corp., New York, NY, 1980.
40. J.D. Hunt: *Mater. Sci. Eng.*, 1984, vol. 65, pp. 75-83.
41. I. Ziv and F. Weinberg: *Metall. Trans. B*, 1989, vol. 20B, pp. 731-34.
42. D.M. Stefanescu, G. Upadhya, and D. Bandyopahyoy: *Metall. Trans. A*, 1990, vol. 21A, pp. 997-1005.